BIOCHEMISTRY
including biophysical chemistry & molecular biology

Article

pubs.acs.org/biochemistry

Atomistic Characterization of the First Step of Calcium Pump Activation Associated with Proton Countertransport

G. Lizbeth Ramírez-Salinas[‡] and L. Michel Espinoza-Fonseca[*,†]

[†]Department of Biochemistry, Molecular Biology and Biophysics, University of Minnesota, Minneapolis, Minnesota 55455, United States

[‡]Laboratorio de Modelado Molecular y Bioinformática, Escuela Superior de Medicina, Instituto Politécnico Nacional, Mexico City 11340, Mexico

ABSTRACT: The calcium pump [sarcoplasmic reticulum (SR) Ca^{2+}-ATPase (SERCA)] transports Ca^{2+} from the cytosol to the SR lumen at the expense of ATP hydrolysis and proton countertransport, thus playing a central role in Ca^{2+} homeostasis and muscle contractility. Proton countertransport via deprotonation of transport site residue Glu309 is a critical first step in SERCA activation because it accelerates the E2−E1 structural transition. Previous studies have suggested that flipping of Glu309 toward the cytosol constitutes the primary mechanism for Glu309 deprotonation, but no conclusive data to support this hypothesis have been published. Therefore, we performed three independent 1 μs molecular dynamics simulations of the E2 state protonated at transport site residues Glu309, Glu771, and Glu908. Structural analysis and pK_a calculations showed that Glu309 deprotonation occurs by an inward-to-outward side-chain transition. We also found that Glu309 deprotonation and proton countertransport occur through transient (~113 ps) water wires connecting Glu309 with the cytosol. Although both mechanisms are operational, we found that transient water wire formation, and not Glu309 flipping, is the primary mechanism for Glu309 deprotonation and translocation of protons to the cytosol. The outward-to-inward transition of protonated Glu309 and the presence of water wires suggest that protons from the cytosol might be passively transported to the lumen via Glu309. However, structural analysis indicates that passive SR proton leakage into the lumen unlikely occurs through Glu309 in the E2 state. These findings provide a time-resolved visualization of the first step in the molecular mechanism of SERCA activation and proton transport across the SR.

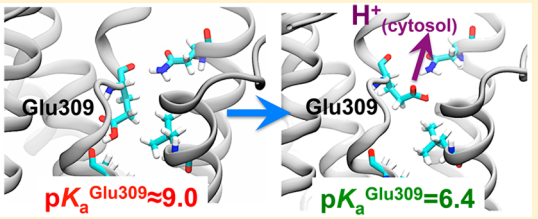

The sarcoplasmic reticulum (SR) Ca^{2+}-ATPase, (SERCA) is a P-type ATPase responsible for clearing cytosolic Ca^{2+} in most cells, thus playing a dominant role in Ca^{2+} homeostasis and muscle contractility.[1] During a single catalytic cycle, SERCA pumps two Ca^{2+} ions into the lumen at the expense of ATP hydrolysis and the countertransport of two protons.[2,3] Each Ca^{2+} transport cycle of SERCA is initiated by deprotonation of transport site residues Glu309 and Glu771 in a low-Ca^{2+} affinity state, E2. The release of protons to the cytosol destabilizes E2 and accelerates the structural transitions toward E1, a high-Ca^{2+} affinity structural state of the pump.[4−6] E1 binds two Ca^{2+} ions to the transport site and one molecule of ATP in the nucleotide-binding cytosolic domain, resulting in a structural arrangement of the pump that is suitable for ATP hydrolysis and autophosphorylation.[6] SERCA then undergoes a structural transition toward a phosphorylated E2 state, thus releasing two Ca^{2+} ions into the SR lumen. The pump becomes dephosphorylated, and two protons are occluded in the transport sites.[7] Finally, SERCA populates the inactive E2 state for the next catalytic cycle.[8]

Proton countertransport via deprotonation of transport site residue Glu309 is the critical first step in SERCA activation because it accelerates the transition from a low-Ca^{2+} affinity state, E2, to a high-Ca^{2+} affinity state, E1 state.[13] Experimental data have shown that at pH >7 in the absence of Ca^{2+}, SERCA predominantly populates the E1, and not the E2, state.[14] This experimental evidence suggests that deprotonation of Glu309 occurs spontaneously at physiological pH. Computational studies have suggested that the side chain of Glu309 undergoes a structural transition between two orientations: a high-pK_a "inward" orientation pointing toward the lumen and a low-pK_a "outward" orientation pointing toward the cytosol (Figure 1).[9,10] On the basis of these findings, it was proposed that flipping of the side chain toward the cytosol is the primary mechanism for Glu309 deprotonation. Although these studies provided for the first time a mechanism for Glu309 deprotonation, the evidence presented in these studies is based on pK_a calculations performed on static crystal structures. Furthermore, these studies did not provide time-resolved information about the dynamics of the Glu309 side chain in solution. Musgaard et al. performed all-atom MD simulations of SERCA to determine the protonation states of transport site residues in the E2 state, but the time scales used in this study (10−50 ns) are probably insufficient to detect side-chain structural transitions between low- and high-pK_a orientations.[15] Alternatively, proton pathways have also been suggested to play a role in E2 deprotonation,[16,17] but these studies did not

Received: June 17, 2015
Revised: August 7, 2015
Published: August 7, 2015

DOI: 10.1021/acs.biochem.5b00672
Biochemistry 2015, 54, 5235−5241

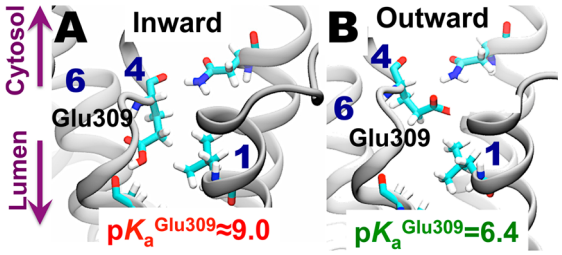

Figure 1. Flipping-induced mechanism for Glu309 deprotonation proposed by Barth and co-workers.[9,10] (A) Inward orientation, in which the side chain of Glu309 points toward the lumen. In this orientation, Glu309 is protonated and interacts with Val304 (B) Glu309 pointing toward the cytosol in an outward orientation. The direct interaction of the carboxylic group with the cytosol favors Glu309 ionization. The average pK_a of Glu309 in each orientation was calculated using PDB entries 2c8k (inward) and 1iwo (outward). pK_a calculations were performed with PROPKA.[11,12] The transmembrane helices are shown as white ribbons and labeled for the sake of clarity. Residues Val304 and Glu309, as well as Leu65 and Asn101, are shown as sticks. The arrows indicate the direction of the lumen and cytosol.

provide direct evidence of the coupling between proton pathway formation and Glu309 ionization. Therefore, the mechanisms by which the E2 state releases a proton from Glu309 under physiological conditions remain unknown. In this study, we used microsecond MD simulations and protein pK_a calculations to determine the mechanisms for Glu309 deprotonation in the E2 state under physiological conditions.

MATERIALS AND METHODS

Molecular Dynamics Simulations. We used three crystal structures of E2 SERCA with a resolution between 0.24 and 0.31 nm as a starting point for our simulations (PDB entries 1iwo,[8] 2agv,[18] and 3w5c[19]). On the basis of previous studies,[15,20] transport site residues E309, E771, and E908 were modeled as protonated, whereas D800 was kept ionized. We adjusted the pK_a of other ionizable residues to simulate SERCA at pH ≈7.0. We inserted each protein in a pre-equilibrated 12 nm × 12 nm POPC bilayer; these lipid−protein systems were solvated using TIP3P water molecules. K^+ and Cl^- ions were added to neutralize the system and to produce a KCl concentration of ∼0.1 M. The final size of the systems was ∼220000 atoms. CHARMM36 force field topologies and parameters were used for the protein, lipid, water, and ions.[21,22]

MD simulations were performed with NAMD 2.9.[23] Simulations were performed at a constant pressure and temperature of 1 atm and 310 K, respectively. We used periodic boundary conditions,[24] the particle mesh Ewald method,[25,26] a nonbonded cutoff of 0.9 nm, and a 2 fs time step. Systems were warmed and equilibrated for 20 ns with backbone atoms harmonically restrained using a force constant of 1000 kcal mol^{-1} nm^{-2}. Production trajectories were performed for 1 μs each, for a total cumulative time of 3 μs.

Protein pK_a Calculations. We used PROPKA 3.1[11,12] to calculate the pK_a values of Glu309 because of flipping of its side chain. PROPKA estimates the empirical pK_a values of ionizable groups in proteins and protein−ligand complexes based on the three-dimensional structure and benefits from explicitly incorporating the Coulombic interactions that arise from mutually titrating residues via the Tanford−Roxby procedure.[27] PROPKA has previously been used to identify the protonation states of acidic residues in SERCA[28,29] and other P-type ATPases, e.g., the Na^+/K^+-ATPase.[30,31]

We also used MCCE[32,33] to calculate changes in Glu309 pK_a induced by the presence of water molecules near its side chain. MCCE uses Monte Carlo sampling to determine side-chain rotamers while keeping the main chain of the protein fixed. The method does not allow the arbitrary definition of the protein dielectric constant; therefore, pK_a calculations in the presence of water wires were performed using the highest dielectric constant allowed by the program (e.g., $\epsilon_{protein}$ = 8.0).

RESULTS

Structural Stability of E2 on the Microsecond Time Scale. We determined the structural stability of the 10-helix transmembrane (TM) domain of E2 SERCA on the microsecond time scale. We measured the time-dependent changes in the root-mean-square deviation (rmsd) of the TM domain for each trajectory (Figure 2). In all three trajectories, the rmsd of

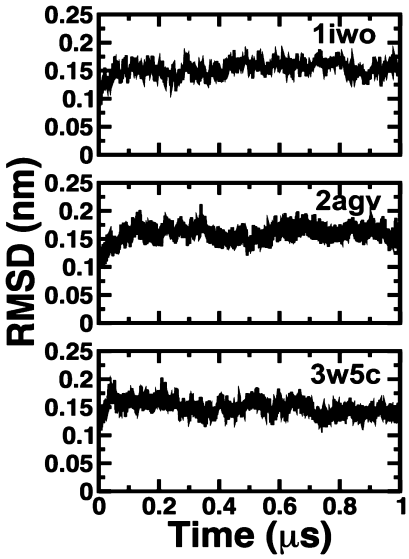

Figure 2. Time-dependent changes in the rmsd of the TM domain of SERCA. Each label indicates the crystal structure used as a starting point for the MD simulations. The rmsd was calculated by superposing only the 10-helix TM domain onto the structure at time zero. The rmsd was calculated at 100 ps time intervals.

the TM domain shifts to a value of ∼0.15 nm but rapidly settles at a plateau on the nanosecond time scale. We also found that the rmsd of the transport sites did not deviate more than 0.2 nm in all trajectories. This small change in rmsd indicates that the geometry of the transport sites in the trajectories is similar to that in the crystal structures. These findings show that in solution, protonation of transport site residues Glu309, Glu771, and Glu908 locks the structure of the TM domain in a structure similar to that in the crystal structures. These observations are in agreement with previous MD studies of the E2 state indicating that protonation of these residues is necessary for the stability of this state.[15,20]

Flipping-Induced Glu309 Deprotonation. Analysis of several crystal structures of E2 showed that the carboxylic group of Glu309 is generally close to the backbone oxygen of Val304 (<0.4 nm) (Table 1). Such a short distance suggests that an orientation of Glu309 pointing toward the lumen is stabilized by a hydrogen bond with Val304. Indeed, protein pK_a

DOI: 10.1021/acs.biochem.5b00672
Biochemistry 2015, 54, 5235−5241

Table 1. Properties of Glu309 in Crystal Structures of E2

PDB entry	$R^{304-309}$ (nm)	pK_a^{309}[a]	orientation
1iwo[8]	0.90	6.4	outward
2avg[18]	0.26	8.7	inward
2ear[34]	0.41	8.3	inward
2eat[34]	0.46	8.7	inward
2c8k[35]	0.29	9.0	inward
2eau[34]	0.33	9.7	inward
3w5c[19]	0.27	9.7	inward

[a] pK_a values were calculated with PROPKA.[11,12]

calculations performed on crystal structures of E2 indicate that Glu309 is protonated when it adopts an inward position (Table 1). However, it has been previously found that Glu309 points outward toward the cytosol in a structure of E2 (PDB entry 1iwo). In this structure, the side chain of Glu309 is located far from Val304 [~0.9 nm (Table 1)] and the carboxylic group is completely exposed to the cytosol. pK_a calculations using this crystal structure showed that flipping of Glu309 from an inward to an outward position is sufficient to decrease the pK_a and promote Glu309 deprotonation (Table 1). This is in agreement with previous studies[9,10] suggesting that spontaneous side-chain flipping deprotonates Glu309. We measured the distance between the hydrogen-bonded carboxylic oxygen of Glu309 and the carbonylic oxygen of Val304 ($R^{309-304}$) to determine whether Glu309 flipping occurs under physiological conditions. We complemented these distance measurements with protein pK_a calculations to determine whether side-chain flipping events lead to Glu309 deprotonation.

To avoid bias against the outward orientation of Glu309 in structure 1iwo, we modeled this residue as protonated. Surprisingly, we found that protonation of this residue shifts toward the occluded conformation during equilibration. This finding indicates that Glu309 pointing toward the lumen is the preferred orientation of Glu309 in E2 SERCA. This finding is in agreement with crystallographic data (Table 1) and with distance measurements between residues Glu309 and Val304. Indeed, we found that Glu309 is hydrogen-bonded to Val304 for >90% of the time in the trajectories (Figure 3A). We also

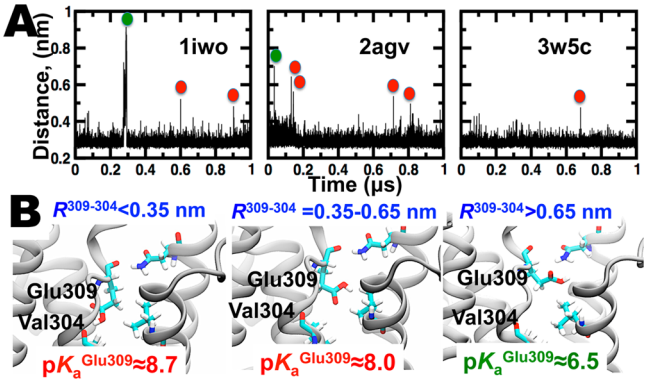

Figure 3. Flipping-induced deprotonation of Glu309. (A) Time evolution of the distance between the carboxylic oxygen of Glu309 and the backbone oxygen of Val304. Red and green ovals indicate partial and complete flipping, respectively, of Glu309 toward the cytosol. (B) Structures of hydrogen-bonded (left), partially flipped (middle), and completely flipped (right) Glu309. The pK_a of Glu309 in each structural arrangement is shown at the bottom of each panel. The TM helices are shown as gray ribbons and individual residues as sticks.

observed transient increases in the distance between Glu309 and Val304. For instance, $R^{309-304}$ in the MD trajectory of 1iwo is ~0.9 and 0.5 nm at 0.29 and 0.6 μs, respectively (Figure 3A). Similar changes in $R^{309-304}$ were observed in the MD trajectories of 2agv and 3w5c. The increase in $R^{309-304}$ is coupled to the flipping of Glu309 toward the cytosol (Figure 3B). Protonated Glu309 adopts three orientations: bound to Val304 (Figure 3B, left), partially flipped (Figure 3B, center), or completely flipped toward the cytosol (Figure 3B, right). We performed protein pK_a calculations with PROPKA[11,12] using representative structures for each orientation to determine whether flipping induces Glu309 deprotonation. Direct interaction with the Val304 backbone oxygen favors Glu309 protonation (Figure 3B, left), in agreement with a recent study by our group.[20] We detected seven partial side-chain flipping events in all trajectories combined [$R^{309-304}$ = 0.35–0.65 nm (Figure 3A, red ovals)]. The pK_a of Glu309 is ~8.0 when its side chain is partially flipped (Figure 3B, middle panel). However, this change in pK_a is not sufficient to deprotonate Glu309 at normal intracellular pH (7.0–7.2).[36,37] Finally, our analysis revealed only two events where Glu309 is completely flipped toward the cytosol (Figure 3A, green ovals). Unlike partial flipping, complete flipping effectively lowers Glu309 pK_a to a value of 6.5 (Figure 2B, right panel), thus favoring deprotonation at physiological pH. Although our structural sampling is limited to the microsecond time scale, our analysis indicates that flipping-induced Glu309 deprotonation occurs infrequently (fewer than one deprotonation event per microsecond) under physiological conditions.

Transient Water Wires Induce Deprotonation of Glu309. Recent studies have revealed the presence of several ion pathways in SERCA,[16] including transient proton release pathways.[38] Therefore, we searched for proton release pathways between Glu309 and the lumen/cytosol in the trajectories of the E2 state. We found the presence of a narrow (0.55 nm in diameter) water pore connecting Glu309 with the cytosol (Figure 4). The pore is formed by the side chains of residues

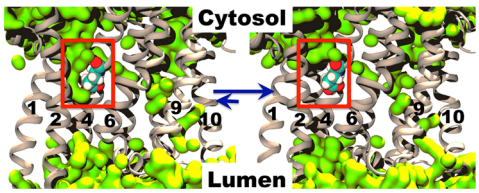

Figure 4. Location of the Glu309–cytosol water pore in E2. The location of the water pore is shown inside the red box; water is shown as a green surface. We found that water molecules transiently reach the carboxylic group of Glu309 (left). However, we found that the equilibrium shifts toward a dry Glu309 conformation (right). The TM helices of SERCA are shown as ribbons. The cytosolic/luminal sides of the membrane and the TM helices are labeled for the sake of clarity.

Glu309, Val62, Leu65, and Leu98. Examination of the water accessibility to this pore revealed that the equilibrium shifts toward a dry Glu309 structure (Figure 4). We detected only between 3 and 10 water pore formation events in each trajectory.

We found that between three and five of the water pore formation events form hydrogen-bonded water wires connecting Glu309 with the cytosol. Three water molecules form each water wire (Figure 5). The average water wire lifetime is ~113 ps (Table 2). We identified two arrangements of water wires:

DOI: 10.1021/acs.biochem.5b00672
Biochemistry 2015, 54, 5235–5241

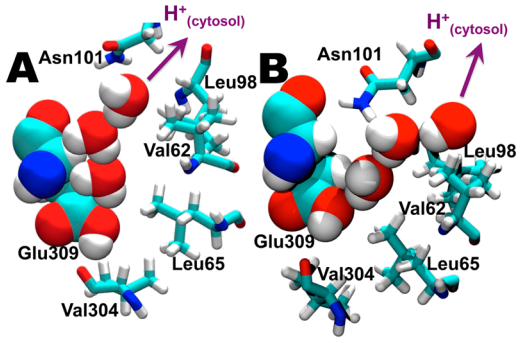

Figure 5. Structure of the water wires linking Glu309 with the cytosol. (A) Geometry of the water wire connecting the carboxylic group of Glu309 with the carboxamide group of Asn101. (B) Structure of the Glu309−cytosol water wire. This geometry is stabilized by the formation of a hydrogen bond between Asn101 and the water molecule in the center of the wire. The arrow indicates the direction of proton translocation. Glu309 and water molecules are shown as spheres; other residues that form the water pore are shown as sticks.

Table 2. Water Wires Detected in the Trajectories

MD trajectory[a]	no. of water wires	water wire lifetime (ps)[b]
1iwo	3	95 ± 32
2agv	5	134 ± 28
3w5c	4	112 ± 38

[a]PDB entries are used as identifiers for each 1 μs trajectory. [b]Reported values are means ± SD.

(i) water wires formed between the carboxyl group of Glu309 and the carboxamide group of Asn101 (Figure 5A) and (ii) a water wire that is stabilized by a hydrogen bond between Asn101 and the water molecule in the center of the wire (Figure 5B). The preference for each water arrangement depends on the presence of a hydrogen bond between the amide moiety of Asn101 and the backbone hydrogen of Glu309 (Figure 3). However, this hydrogen bond does not interfere with the stability of the water wires.

We used MCCE[32,33] to calculate the changes in pK_a of Glu309 induced by the formation of water wires. In the presence of these transient water wires, Glu309 has pK_a values between 6.2 and 6.5. This indicates that these transient water wires promote deprotonation of Glu309. Although we did not explicitly include protons in our simulation, previous computational studies of proton translocation through water wires indicate that an average lifetime of 100 ps is required for protons to permeate a 3 nm channel.[39] Therefore, we propose that these water wires facilitate the translocation of protons to the cytosol via Grotthuss shuttling[39,40] because the water wires are much shorter (<1 nm) and form within the 100 ps lifetime range required for proton translocation.

Effects of Deprotonation on the Structural Dynamics of Glu309. We found that both water wire formation and Glu309 flipping can contribute to Glu309 deprotonation. However, our MD simulations were performed in the presence of an explicit proton bound to Glu309. Therefore, an important question arises from our findings: Does Glu309 fluctuate between inward and outward orientations upon deprotonation? We performed three 0.5 μs MD simulations of E2 SERCA in the absence of a proton at Glu309 to address this issue. We used three different structures as a starting point for these simulations: (i) crystal structure 1iwo, in which Glu309 points toward the cytosol in this crystal structure, (ii) a structure extracted from trajectory 2agv at 0.04 μs (Figure 3A, middle panel), and (iii) a representative structure of 3w5c in which a water wire connects Glu309 with the cytosol. We found that during equilibration, deprotonated Glu309 remains in an outward orientation. In the cases in which Glu309 initially adopts an inward conformation, Glu309 rapidly separates from Val304 upon deprotonation and rapidly flips toward the outward orientation during equilibration (10 ns). This finding is not surprising because proton removal induces electrostatic repulsion between the negatively charged carboxylic group of Glu309 and the backbone oxygen of Val304.

To further determine whether deprotonated Glu309 undergoes a reversible inward-to-outward transition similar to that of protonated Glu309, we measured the distance between Glu309 and Val304 (Figure 6). In general, we found that Glu309 and

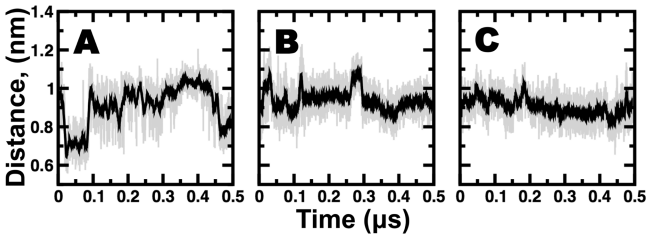

Figure 6. Effects of Glu309 deprotonation on the Glu309−Val304 distance. (A) Time evolution of the distance between the carboxylic oxygen of Glu309 and the backbone oxygen of Val304 using crystal structure 1iwo as a starting structure. (B) Changes in the Glu309−Val304 distance upon deprotonation of a structure extracted from trajectory 2agv at 0.04 μs (Figure 1A, middle panel). (C) Distances between Glu309 and Val304 in a trajectory starting from a representative structure of 3w5c in which a water wire connects Glu309 with the cytosol. The raw data are colored gray, and the time-averaged data sampled every 1 ns are colored black.

Val304 are separated by at least 0.8 nm (Figure 6), indicating that deprotonated Glu309 adopts an outward orientation pointing toward the cytosol. However, we found that the distance between Glu309 and Val304 in the trajectory starting from crystal structure 1iwo decreases by ~0.3 nm between 0.02 and 0.1 μs, as well as between 0.45 and 0.5 μs and in the simulation (Figure 6A). This change is coupled to a partial transition of Glu309 toward an inward orientation pointing to the lumen. Although protein pK_a calculations indicate that Glu309 is deprotonated in this partially flipped orientation, it is possible that Glu309 may sequester a proton from the cytosol to adopt a high-pK_a orientation (Figure 3B). Nevertheless, our data indicate that although outward-to-inward flipping of deprotonated Glu309 occurs in solution, Glu309 primarily adopts an outward orientation pointing toward the cytosol.

■ DISCUSSION

Early computational studies have suggested that the primary mechanism for Glu309 deprotonation is the structural transition between inward (high-pK_a) and outward (low-pK_a) orientations of Glu309.[9,10] However, the MD trajectories in this study revealed not one but two mechanisms for Glu309 deprotonation: Glu309 flipping and water wire formation between Glu309 and the cytosol. Our findings indicate that Glu309 flipping and water wire formation are two events that occur independently. For instance, water wire formation does not initiate flipping of Glu309 toward the cytosol; in fact, Glu309 flipping occurs most effectively when the region of

DOI: 10.1021/acs.biochem.5b00672
Biochemistry 2015, 54, 5235−5241

SERCA surrounding Glu309 is devoid of water molecules. We found that in solution, both mechanisms for Glu309 are operational in SERCA. However, our data suggest that Glu309 flipping is not the primary mechanism for Glu309 ionization. Indeed, we found that Glu309 flipping and water wire formation deprotonate Glu309 at a relative rate of 0.7 and 3 ionization events per microsecond, respectively. These relative rates are based on 1 μs simulations, so the results should be interpreted with caution; these numbers would probably change significantly if the simulations were extended. Nevertheless, these relative rates indicate that water wire formation occurs more frequently than side-chain flipping. Therefore, we propose that water wire formation is the primary mechanism for Glu309 deprotonation and countertransport of protons to the cytosol. The relative rate for Glu309 deprotonation through water wire formation occurs on the microsecond time scale, much faster than the rate of ATP-dependent calcium transport molecular turnover by SERCA (~30 Ca^{2+} ions per SERCA molecule per second). Therefore, Glu309 deprotonation is independent of ATP hydrolysis, thus shifting the equilibrium toward the high-Ca^{2+} affinity E1 state under physiological conditions.[14] These observations indicate that the time scale for Glu309 deprotonation found in the MD trajectories occurs within a physiological window.

Previous studies have suggested the presence of at least two ion pathways in SERCA that can be used for proton countertransport. Hauser and Barth proposed that Glu309 serves as a proton shuttle between the transport site and the cytosol.[9] On the other hand, Bublitz et al. have suggested that the E2 state has two cytosolic pathways located near the N- and C-termini of the TM helices working in concert.[16] The authors have suggested that metal ions and protons are transported primarily through the N-terminal and C-terminal pathways, respectively. Therefore, the question of which pathway is the primary pathway for proton countertransport in E2 arises from our simulations. A recent study of the proton pump showed that a conserved residue, Asn106, plays a central role in proton occlusion via interaction with residue Asp684.[41] Studies of protonation and/or deprotonation of Asp96, the proton donor to the Schiff base in the $M_2' \rightarrow N$ reaction in bacteriorhodopsin, have shown that replacement of Asp96 with an asparagine makes the proton transfer very slow and pH-dependent.[42−44] These studies suggest that while protons could be transported from Glu771 to Glu309, Asn796 likely increases the energetic barrier for proton transfer, thus substantially decreasing the rate of translocation of protons to the cytosol. Therefore, it is unlikely that proton countertransport occurs primarily through Glu309 via Asn796.[9,17] Instead, we propose that while the release of a proton from Glu309 occurs through the N-terminal region of the TM domain, proton countertransport from the transport site residue Glu771/Glu908 likely occurs through a C-terminal pathway proposed by Bublitz et al.[16] This C-terminal pathway proposed by Bublitz et al.[16] and confirmed by our studies (Figure 4) is completely open in E2, thus providing a proton translocation pathway that is virtually barrierless. In this case, proton countertransport from Glu771/Glu908 to the cytosol via the C-terminal pathway is probably coupled to binding of a metal ion to these residues from the N-terminal pathway,[16] thus facilitating countertransport of two protons coupled to the E2−E1 transition.[2,3]

Finally, previous studies have shown that the SR membrane is permeable to protons, and that proton leakage accounts for 5−10% of the necessary charge compensation during the release of calcium to the cytosol.[45] We have recently suggested that SERCA has the ability to passively transport protons toward the lumen using an inhibited E1 intermediate state protonated at Glu771, $E1{\cdot}H^{+}_{771}$. In this intermediate, water wires form between transport site residue Glu908 and the lumen, thus providing a unidirectional proton pathway toward the lumen.[38] Our simulations revealed that protonated Glu309 undergoes an outward-to-inward side-chain transition; therefore, proton shuttling from the cytosol to the lumen might occur through E2. However, it is unlikely that passive proton transport occurs in the E2 state via Glu309 because (i) protons might encounter a large energy barrier along the Glu771/Asn796 pathway and (ii) unlike $E1{\cdot}H^{+}_{771}$, we did not observe the presence of simultaneous cytosolic and luminal pathways necessary for translocation of protons to the lumen.

CONCLUSION

In conclusion, we used microsecond atomistic simulations to identify the mechanisms for Glu309 deprotonation in the E2 state of SERCA. Structural analysis and pK_a calculations showed that Glu309 deprotonation occurs by an inward-to-outward side-chain transition. We also found that Glu309 deprotonation and proton countertransport occur through transient (~113 ps) water wires connecting Glu309 with the cytosol. Although both mechanisms are operational, we found that transient water wire formation, and not Glu309 flipping, is the primary mechanism for Glu309 deprotonation and translocation of protons to the cytosol. The outward-to-inward transition of protonated Glu309 and the presence of water wires suggest that protons from the cytosol might be passively transported to the lumen via Glu309. However, structural analysis indicates that that passive SR proton leakage into the lumen unlikely occurs through Glu309. These findings provide a time-resolved visualization of the first step in the molecular mechanism of SERCA activation and proton transport across the SR membrane.

AUTHOR INFORMATION

Corresponding Author

*E-mail: espin049@umn.edu.

Funding

This work was supported by a grant from the American Heart Association to L.M.E.-F. (Grant 12SDG12060656). G.L.R.-S. is supported by a predoctoral fellowship from CONACYT-Mexico.

Notes

The authors declare no competing financial interest.

ACKNOWLEDGMENTS

We thank Joseph M. Autry for many helpful discussions. This project made extensive use of the outstanding high-performance computing facilities at the Minnesota Supercomputing Institute.

ABBREVIATIONS

SERCA, sarcoplasmic reticulum Ca^{2+}-ATPase; SR, sarcoplasmic reticulum; MD, molecular dynamics; TM, transmembrane; rmsd, root-mean-square deviation; PDB, Protein Data Bank; POPC, 1-palmitoyl-2-oleoyl-*sn*-glycero-3-phosphocholine; TIP3P, transferable intermolecular potential, three-point; CHARMM36, Chemistry at HARvard Macromolecular Mechanics force field, version c36; SD, standard deviation.

DOI: 10.1021/acs.biochem.5b00672
Biochemistry 2015, 54, 5235−5241

REFERENCES

(1) Periasamy, M., and Huke, S. (2001) SERCA pump level is a critical determinant of Ca(2+)homeostasis and cardiac contractility. *J. Mol. Cell. Cardiol. 33*, 1053−1063.

(2) Yu, X., Carroll, S., Rigaud, J. L., and Inesi, G. (1993) H+ countertransport and electrogenicity of the sarcoplasmic reticulum Ca2+ pump in reconstituted proteoliposomes. *Biophys. J. 64*, 1232−1242.

(3) Zafar, S., Hussain, A., Liu, Y., Lewis, D., and Inesi, G. (2008) Specificity of ligand binding to transport sites: Ca2+ binding to the Ca2+ transport ATPase and its dependence on H+ and Mg2+. *Arch. Biochem. Biophys. 476*, 87−94.

(4) Bublitz, M., Poulsen, H., Morth, J. P., and Nissen, P. (2010) In and out of the cation pumps: P-type ATPase structure revisited. *Curr. Opin. Struct. Biol. 20*, 431−439.

(5) Toyoshima, C. (2009) How Ca2+-ATPase pumps ions across the sarcoplasmic reticulum membrane. *Biochim. Biophys. Acta, Mol. Cell Res. 1793*, 941−946.

(6) Toyoshima, C., and Mizutani, T. (2004) Crystal structure of the calcium pump with a bound ATP analogue. *Nature 430*, 529−535.

(7) Olesen, C., Sorensen, T. L., Nielsen, R. C., Møller, J. V., and Nissen, P. (2004) Dephosphorylation of the calcium pump coupled to counterion occlusion. *Science 306*, 2251−2255.

(8) Toyoshima, C., and Nomura, H. (2002) Structural changes in the calcium pump accompanying the dissociation of calcium. *Nature 418*, 605−611.

(9) Hauser, K., and Barth, A. (2007) Side-chain protonation and mobility in the sarcoplasmic reticulum Ca2+-ATPase: implications for proton countertransport and Ca2+ release. *Biophys. J. 93*, 3259−3270.

(10) Andersson, J., Hauser, K., Karjalainen, E. L., and Barth, A. (2008) Protonation and hydrogen bonding of Ca2+ site residues in the E2P phosphoenzyme intermediate of sarcoplasmic reticulum Ca2+-ATPase studied by a combination of infrared spectroscopy and electrostatic calculations. *Biophys. J. 94*, 600−611.

(11) Olsson, M. H. M., Søndergaard, C. R., Rostkowski, M., and Jensen, J. H. (2011) PROPKA3: Consistent Treatment of Internal and Surface Residues in Empirical pK(a) Predictions. *J. Chem. Theory Comput. 7*, 525−537.

(12) Søndergaard, C. R., Olsson, M. H. M., Rostkowski, M., and Jensen, J. H. (2011) Improved Treatment of Ligands and Coupling Effects in Empirical Calculation and Rationalization of pK(a) Values. *J. Chem. Theory Comput. 7*, 2284−2295.

(13) Inesi, G., Lewis, D., Toyoshima, C., Hirata, A., and de Meis, L. (2008) Conformational fluctuations of the Ca2+-ATPase in the native membrane environment. Effects of pH, temperature, catalytic substrates, and thapsigargin. *J. Biol. Chem. 283*, 1189−1196.

(14) Tadini-Buoninsegni, F., Bartolommei, G., Moncelli, M. R., Guidelli, R., and Inesi, G. (2006) Pre-steady state electrogenic events of Ca2+/H+ exchange and transport by the Ca2+-ATPase. *J. Biol. Chem. 281*, 37720−37727.

(15) Musgaard, M., Thøgersen, L., and Schiøtt, B. (2011) Protonation states of important acidic residues in the central Ca(2)(+) ion binding sites of the Ca(2)(+)-ATPase: a molecular modeling study. *Biochemistry 50*, 11109−11120.

(16) Bublitz, M., Musgaard, M., Poulsen, H., Thogersen, L., Olesen, C., Schiott, B., Morth, J. P., Møller, J. V., and Nissen, P. (2013) Ion pathways in the sarcoplasmic reticulum Ca2+-ATPase. *J. Biol. Chem. 288*, 10759−10765.

(17) Karjalainen, E. L., Hauser, K., and Barth, A. (2007) Proton paths in the sarcoplasmic reticulum Ca(2+) -ATPase. *Biochim. Biophys. Acta, Bioenerg. 1767*, 1310−1318.

(18) Obara, K., Miyashita, N., Xu, C., Toyoshima, I., Sugita, Y., Inesi, G., and Toyoshima, C. (2005)) Structural role of countertransport revealed in Ca(2+) pump crystal structure in the absence of Ca(2+). *Proc. Natl. Acad. Sci. U. S. A. 102*, 14489−14496.

(19) Toyoshima, C., Iwasawa, S., Ogawa, H., Hirata, A., Tsueda, J., and Inesi, G. (2013) Crystal structures of the calcium pump and sarcolipin in the Mg2+-bound E1 state. *Nature 495*, 260−264.

(20) Espinoza-Fonseca, L. M., Autry, J. M., Ramirez-Salinas, G. L., and Thomas, D. D. (2015) Atomic-level mechanisms for phospholamban regulation of the calcium pump. *Biophys. J. 108*, 1697−1708.

(21) Best, R. B., Zhu, X., Shim, J., Lopes, P. E., Mittal, J., Feig, M., and Mackerell, A. D., Jr. (2012) Optimization of the additive CHARMM all-atom protein force field targeting improved sampling of the backbone phi, psi and side-chain chi(1) and chi(2) dihedral angles. *J. Chem. Theory Comput. 8*, 3257−3273.

(22) MacKerell, A. D., Jr., Feig, M., and Brooks, C. L., 3rd. (2004) Improved treatment of the protein backbone in empirical force fields. *J. Am. Chem. Soc. 126*, 698−699.

(23) Phillips, J. C., Braun, R., Wang, W., Gumbart, J., Tajkhorshid, E., Villa, E., Chipot, C., Skeel, R. D., Kale, L., and Schulten, K. (2005) Scalable molecular dynamics with NAMD. *J. Comput. Chem. 26*, 1781−1802.

(24) Weber, W., Hünenberger, P. H., and McCammon, J. A. (2000) Molecular Dynamics Simulations of a Polyalanine Octapeptide under Ewald Boundary Conditions: Influence of Artificial Periodicity on Peptide Conformation. *J. Phys. Chem. B 104*, 3668−3675.

(25) Darden, T., York, D., and Pedersen, L. (1993) Particle mesh Ewald: An N·log(N) method for Ewald sums in large systems. *J. Chem. Phys. 98*, 10089−10092.

(26) Essmann, U., Perera, L., Berkowitz, M. L., Darden, T., Lee, H., and Pedersen, L. G. (1995) A smooth particle mesh Ewald method. *J. Chem. Phys. 103*, 8577−8593.

(27) Tanford, C., and Roxby, R. (1972) Interpretation of protein titration curves. Application to lysozyme. *Biochemistry 11*, 2192−2198.

(28) Espinoza-Fonseca, L. M., Autry, J. M., Ramirez-Salinas, G. L., and Thomas, D. D. (2015) Atomic-level mechanisms for phospholamban regulation of the calcium pump. *Biophys. J. 108*, 1697−1708.

(29) Espinoza-Fonseca, L. M., Autry, J. M., and Thomas, D. D. (2015) Sarcolipin and phospholamban inhibit the calcium pump by populating a similar metal ion-free intermediate state. *Biochem. Biophys. Res. Commun. 463*, 37−41.

(30) Cornelius, F., Kanai, R., and Toyoshima, C. (2013) A Structural View on the Functional Importance of the Sugar Moiety and Steroid Hydroxyls of Cardiotonic Steroids in Binding to Na,K-ATPase. *J. Biol. Chem. 288*, 6602−6616.

(31) Yu, H. B., Ratheal, I. M., Artigas, P., and Roux, B. (2011) Protonation of key acidic residues is critical for the K+-selectivity of the Na/K pump. *Nat. Struct. Mol. Biol. 18*, 1159−U1116.

(32) Alexov, E. G., and Gunner, M. R. (1997) Incorporating protein conformational flexibility into the calculation of pH-dependent protein properties. *Biophys. J. 72*, 2075−2093.

(33) Georgescu, R. E., Alexov, E. G., and Gunner, M. R. (2002) Combining conformational flexibility and continuum electrostatics for calculating pK(a)s in proteins. *Biophys. J. 83*, 1731−1748.

(34) Takahashi, M., Kondou, Y., and Toyoshima, C. (2007) Interdomain communication in calcium pump as revealed in the crystal structures with transmembrane inhibitors. *Proc. Natl. Acad. Sci. U. S. A. 104*, 5800−5805.

(35) Jensen, A. M., Sørensen, T. L., Olesen, C., Møller, J. V., and Nissen, P. (2006) Modulatory and catalytic modes of ATP binding by the calcium pump. *EMBO J. 25*, 2305−2314.

(36) Pan, J. W., Hamm, J. R., Rothman, D. L., and Shulman, R. G. (1988) Intracellular pH in human skeletal muscle by 1H NMR. *Proc. Natl. Acad. Sci. U. S. A. 85*, 7836−7839.

(37) Steenbergen, C., Deleeuw, G., Rich, T., and Williamson, J. R. (1977) Effects of acidosis and ischemia on contractility and intracellular pH of rat heart. *Circ. Res. 41*, 849−858.

(38) Espinoza-Fonseca, L. M., and Ramirez-Salinas, G. L. (2015) Microsecond Molecular Simulations Reveal a Transient Proton Pathway in the Calcium Pump. *J. Am. Chem. Soc. 137*, 7055−7058.

(39) Brewer, M. L., Schmitt, U. W., and Voth, G. A. (2001) The formation and dynamics of proton wires in channel environments. *Biophys. J. 80*, 1691−1702.

(40) Wu, Y., Ilan, B., and Voth, G. A. (2007) Charge delocalization in proton channels, II: the synthetic LS2 channel and proton selectivity. *Biophys. J. 92*, 61−69.

DOI: 10.1021/acs.biochem.5b00672
Biochemistry 2015, 54, 5235−5241

(41) Ekberg, K., Wielandt, A. G., Buch-Pedersen, M. J., and Palmgren, M. G. (2013) A conserved asparagine in a P-type proton pump is required for efficient gating of protons. *J. Biol. Chem. 288*, 9610−9618.
(42) Cao, Y., Varo, G., Chang, M., Ni, B. F., Needleman, R., and Lanyi, J. K. (1991) Water is required for proton transfer from aspartate-96 to the bacteriorhodopsin Schiff base. *Biochemistry 30*, 10972−10979.
(43) Gerwert, K., Hess, B., Soppa, J., and Oesterhelt, D. (1989) Role of aspartate-96 in proton translocation by bacteriorhodopsin. *Proc. Natl. Acad. Sci. U. S. A. 86*, 4943−4947.
(44) Otto, H., Marti, T., Holz, M., Mogi, T., Lindau, M., Khorana, H. G., and Heyn, M. P. (1989) Aspartic acid-96 is the internal proton donor in the reprotonation of the Schiff base of bacteriorhodopsin. *Proc. Natl. Acad. Sci. U. S. A. 86*, 9228−9232.
(45) Kamp, F., Donoso, P., and Hidalgo, C. (1998) Changes in luminal pH caused by calcium release in sarcoplasmic reticulum vesicles. *Biophys. J. 74*, 290−296.

DOI: 10.1021/acs.biochem.5b00672
Biochemistry 2015, 54, 5235−5241